PSFC/JA-10-20

VUV Impurity Spectroscopy on the Alcator C-Mod Tokamak

Reinke, M.L., *Beiersdorfer, P., Howard, N. T., *Magee, E.W., Podpaly, Y., Rice, J.E., Terry, J.L.

*Physics Division, Lawrence Livermore National Laboratory, Livermore, CA

January 2011

Plasma Science and Fusion Center
Massachusetts Institute of Technology
Cambridge MA 02139 USA

This work was supported by the U.S. Department of Energy, Contract No. DE-FC0299ER54512 and DE-AC52-07NA-27344.

VUV Impurity Spectroscopy on the Alcator C-Mod Tokamak[a]

M. L. Reinke,[1,b] P. Beiersdorfer,[2] N. T. Howard,[1] E. W. Magee,[2] Y. Podpaly,[1] J. E. Rice,[1] and J. L. Terry[1]

[1]*Plasma Science and Fusion Center, MIT, Cambridge, MA*
[2]*Physics Division, Lawrence Livermore National Laboratory, Livermore, CA*

Vacuum ultraviolet (VUV) spectroscopy is used on the Alcator C-Mod tokmak to study the physics of impurity transport and provide feedback on impurity levels to assist experimental operations. Sputtering from C-Mod's all metal (Mo+W) plasma facing components and ICRF antenna and vessel structures (sources for Ti, Fe, Cu and Ni), the use of boronization for plasma surface conditioning and Ar, Ne or N_2 gas seeding combine to provide a wealth of spectroscopic data from low-Z to high-Z. Recently, a laser blow-off impurity injector has been added, employing CaF_2 to study core and edge impurity transport. One of the primary tools used to monitor the impurities is a 2.2 meter Rowland circle spectrometer utilizing a Reticon array fiber coupled to a microchannel plate. With a 600 lines/mm grating the $80 < \lambda < 1050$ Å range can be scanned, although only 40-100 Å can be observed for a single discharge. Recently, a flat-field grating spectrometer was installed which utilizes a varied line spacing grating to image the spectrum to a soft x-ray sensitive Princeton Instruments CCD camera. Using a 2400 lines/mm grating, the $1\ 0< \lambda < 70$ Å range can be scanned with 5-6 nm observed for a single discharge. A variety of results from recent experiments are shown that highlight the capability to track a wide range of impurities.

I. INTRODUCTION

Alcator C-Mod[1] is a compact, R ~ 0.68 m, high field, $B_t < 8$ T, high density, $n_e < 10^{21}$ m^{-3}, high temperature, $T_e < 9$ keV, tokamak used to investigate a wide range of plasma physics and fusion engineering topics. As with most high temperature plasma devices, C-Mod's vacuum ultraviolet (VUV) spectroscopy tools fulfill both operations and physics goals. Impurity monitoring helps to identify the presence of contaminants that might indicate unexpected and unwanted deterioration of in-vessel components. This provides useful feedback to ensure efficient and safe utilization of the tokamak. Impurities are also purposefully injected into the plasma and the transient response tracked to study the physics of both turbulent and neoclassical particle transport. Observations from both intentionally and unintentionally seeded impurities also supports research on atomic processes in high temperature plasmas. This paper describes the tools and methods used to accomplish these goals on Alcator C-Mod, highlighting results from a newly installed flat-field VUV spectrometer.

II. DESCRIPTION OF DIAGNOSTIC TOOLS

VUV spectroscopy on C-Mod is performed using two instruments, a 2.2 meter, grazing-incidence Rowland circle spectrometer and a compact flat-field spectrometer. The Rowland circle spectrometer[2,3] one of the original C-Mod diagnostics, is a McPherson Model 247 using a 600 l/mm grating. Although a wide wavelength region of 90-1030 Å can be scanned shot-to-shot, only 40-100 Å can be observed at a time with $d\lambda/\lambda \sim 100$ resolving power. The dispersed light is incident on a micro-channel plate image intensifier which is then fiber coupled to a 1024-ch RL 1024S Reticon photodiode array. Full spectra can be collect up to 250 Hz with a region of interest observed at up to 2 kHz. The spectrometer views the plasma on a poloidal plane with a line-of sight that can be scanned on a shot-to-shot basis, using repeatable shots to measure a radial brightness profile.

The second instrument, installed during the FY10 run campaign, is a flat-field grating spectrometer. This instrument, developed by LLNL for use on EBIT-I is identical in working principles to the X-ray and Extreme Ultraviolet Spectrometer (XEUS) recently installed on NSTX[4] and so we have continued with this naming convention at C-Mod. XEUS uses a varied line spacing (VLS) grating which compresses a a large portion of the Rowland circle to a flat focal plane allowing wide spectrum monitoring in a single instrument. The LLNL designed 2400 l/mm grating is functionally identical to a VLS Hitachi grating used in the XEUS on NSTX as well as other high temperature plasma experiments[5,6]. The spectrometer's 100 μm entrance slit is located approximately 4.0 meters from center of the tokamak and the slit/grating and grating/detector distance are both approximately 25 cm . The instrument's line of sight impacts the major axis of the plasma at the midplane with a slight downward angle of 6.5° and is collimated by at 2 m long, 3.8 cm diameter tube connecting the exit of the spectrometer to the vacuum vessel. This results in a ~7 cm vertically extended observation volume on axis. The dispersed photons are observed directly using a Princeton Instruments PIXIS-XO 100B camera with a 1340 x 100 back-illuminated CCD designed for use with SXR/VUV light. No shutter is used so there is a small amount of temporal smearing but the pixel rows have been aligned parallel to the dispersion plane in order to minimize

[a]Contributed paper published as part of the Proceedings of the 18th Topical Conference on High-Temperature Plasma Diagnostics, Wildwood, New Jersey, May, 2010.
[b]Author to whom correspondence should be addressed. Electonic mail: mlreinke@psfc.mit.edu

spectral smearing during readout. Micrometers can be used to adjust the CCD camera's position and orientation relative to the grating, changing the wavelength coverage and focus of the spectra. These VLS suffer from non-linear dispersion and to calibrate the wavelength scale, a 2nd order polynomial is fit to the pixel locations for distinct, well known lines. The small height of the CCD, 33 kHz row shift rate and 2 MHz digitization rate allow for fast framing times, and spectra are routinely collected with time resolution of approximately 5 ms. This is over an order of magnitude faster then previously achieved[4] and enables transient impurity transport to be investigated as discussed in Section IV. To increase signal without sacrificing time resolution, on-chip binning is used to combine multiple rows into a single spectrum prior to digitization. Typically between 20 to 40 rows are used to reach near ½ scale on the CCD for the B V Ly-α, corresponding to a photon flux at the camera of nearly 3.0×10^{13} ph/s/m^2.

III. IMPURITY MONITORING

Alcator C-Mod uses solid Mo and W tiles for plasma facing components (PFCs) in the divertor and inner and outer limiters. Auxiliary heating is provided by three ion cyclotron range of frequency (ICRF) antennae constructed from a variety of materials. The limiters are made of Mo, straps are Cu-coated INCONEL 625 (60% Ni, 20% Cr) and the Faraday screens are TiC-coated INCONEL. The vacuum vessel and many in-vessel structures are made from 304 stainless steel[7]. Contamination of the plasma by one or more of these impurities can lead to significant radiative power loss so most of these materials are continuously monitored and shot-to-shot feedback is provided to experimental leaders. We accomplish this using the Rowland circle spectrometer observing the 100-140 Å spectral region as shown in Figure 1. The primary feature of interest is the 3s-3p Na-like and $3s^2$-3s3p Mg-like Mo lines at 127.8 Å and 116.0 Å which can be easily modeled to provide quantitative Mo density[3]. Also within this range are $2s^2$-2s2p Be-like lines from Fe, Ni and Cu (not shown). The line-integrated brightness is enhanced by also observing $2s^22p^3$-$2s2p^4$ N-like emission which is nearly degenerate with the Be-like emission for Fe, Ni and Cu. From Ar to Kr, the energy difference between the N-like and Be-like lines changes from -0.77 eV to 2.1 eV, crossing zero near Z=24 at Cr. While the sum of these two lines increases the SNR for impurity identification, depending on electron temperature and transport, relative abundance of each charge state can vary making it necessary to model both lines to accurately estimate impurity densities. Ti injections can be identified via several M-shell and L-shell transitions in this spectral region, with the high-n Na-like Ti XII lines at 115.0 Å the most unambiguous sign, but these lines have proven difficult to quantitatively model. In the most recent run campaign, melting of W PFCs in the divertor has required C-Mod to monitor W contamination as well. Figure 1 shows the spectrum from the Rowland circle spectrometer before and after an unintentional injection of W into the core plasma. Although the 125-135 Å region has been used on ASDEX-U[8], many lines overlap with emission from other impurities. Most notably the strong 132.9 Å Zn-like W line is degenerate with the Be-like Fe line. Additionally, bright Cu-like and Ga-like W lines between 126-130 Å are obscured by the Na-like Mo lines. The quasicontinuum and line emission from tungsten in the 40-60 Å region observed by XEUS is being investigated as a more reliable W impurity density measurement.

To help mitigate the sputtering of Mo frm PFCs, a low-Z coating is applied by injecting diborane (B_2D_6) into an electron cyclotron discharge[9] which results in boron being the most abundant impurity at approximately a $n_z/n_e \sim 0.01$ level. Prior to the first boronization after an opening C and O, are observed but generally are not a concern for most plasmas. Fluorine is the next most abundant low-Z impurity at a level of a fraction of percent. The specific source of F has not been identified but is thought to be from evaporation from the numerous sources of Teflon used in vacuum-compatible cables. To reduce the heat flux to PFCs via radiation, Ne and N_2 have been used in some high power ICRF experiments. These low-Z elements are observed via K-shell emission in the 10-60 Å region by XEUS. Figure 5 and 6 show the H-like and He-like B and N spectra at multiple n-numbers. The enhancement of the high-n spectra is discussed in Section V. The low-n emission lines such as Ly-α or Ly-β can be easily modeled using data from OPEN-ADAS to provide quantitative low-Z impurity density measurements.

IV. IMPURITY TRANSPORT

A new laser blow-off (LBO) system has recently been installed on C-Mod for impurity transport studies. A wide range of materials from carbon to tungsten has been injected, although most studies have used CaF_2 in order to simultaneously study core (Ca) and edge (F) transport in Ohmic, L-mode and H-mode plasmas[10]. The Ca can be tracked using L-shell emission from the Li-, Be- and B-like isoelectronic sequences. Since experimentally verified energy level data on highly ionized Ca in this spectral range is limited, the dominant iso-electronic features were observed and identified using Ar. HULLAC modeling confirmed by EBIT-II measurements have identified contributions from Ne-like to Li-like Ar within the XEUS spectral range[11]. Ar was seeded into an Ohmic plasma with a core electron temperature of 2 keV and the observed spectrum shown in Figure 2. In this temperature range, the Li-, Be- and B-Like lines are the most distinct lines and are listed in Table 1. CaF_2 was injected into an ICRF-heated L-mode plasma with a core temperature of 3.1 keV and the change in spectrum seen by XEUS is plotted in Figure 3. Qualitatively comparing the two impurities shows the same features dominate the spectrum as would be expected for such a small change in atomic number. Ca wavelengths[12] for the transitions identified from the Ar spectrum show good agreement with the measurements. The time evolution of the 1s-2p F IX and 2s-3p Ca XVIII lines are shown in Figure 4 along with the 1s-2p O VIII which must be included in a two-peak fit with the Ca XVIII line. The green box shows the time points averaged together to form the spectrum plotted in Figure 3 with the background taken from the frame before the impurity injection at 0.95 seconds. The time resolution of the diagnostic is able to resolve the 20-30 ms impurity confinement time typical of turbulent impurity transport in tokamaks. Additionally, the time evolution of H-like F is different from Li-like Ca, with the Ca emission peaking ~15 ms later than the F and the background H-like O shows no variation with time. These data will constrain radial impurity transport simulations which takes into account the ionization and recombination physics of each impurity. Although lower charge states of Ca are observable for $\lambda > 23$ Å, Ar is regularly used for x-ray crystal spectroscopy measurements and the brighter Ar L-shell emission prevents these charge states of Ca from being quantitatively useful because of overlap.

V. IMPACT OF CHARGE-EXCHANGE ON THE LYMAN SERIES OF LOW-Z ELEMENTS

The XEUS spectrometer is able to resolve the Lyman series of low-Z impurities and a enhancement in the high-n line emission has been observed for H-like B and N. When the excited state populations for H-like ions are determined by electron impact processes alone, the relative brightness of the high-n transitions should fall off approximately by $1/n^3$ as shown previously for carbon[13]. In the C-Mod spectra for B V and N VII shown in Figures 5 and 6, respectively, such a fall off is routinely not observed. For B V, the Ly_γ brightness is greater than Ly_β and for N VII Ly_δ is greater than Ly_γ. At C-Mod plasma temperatures, these charge states will be present out near the edge of the plasma where the neutral hydrogen density is higher, enhancing charge-exchange effects relative to electron imapct processes. For boron, *nl*-resolved charge-exchange cross-sections at thermal impact energies have been generated using the quantal formalism[14]. These results show that at low-energies, down to 250 eV/amu, the cross-section peaks strongly at n=4 and is more than 100 times higher than either of the n=5 or n=3 cross-sections. This indicates that state-selective charge-exchange is consistent with the distortion seen by XEUS. For the N VII Lyman series, the enhancements occurs for at n=5, higher then for boron, as expected, although neither follow the $n_{peak} \sim Z^{3/4}$ scaling commonly cited[15]. The effect of charge-exchange on the Lyman series of C VI has been observed previously on JET[13,15] but the distortion is not nearly as pronounced and the line brightness monotonically decreases as n increases. In the future, quantitative population modeling including both electron impact processes and charge-exchange will be used to allow for more rigorous conclusions. In addition, thermal charge-exchange cross-sections reactions involving N^{7+} need to be calculated using the quantal method as done for B^{5+}. This technique is currently utilized on C-Mod to study flow physics on the high-field side of the tokamak where the diagnostic neutral beam cannot penetrate[16].

V. CONCLUSIONS

A flat-field SXR/VUV spectrometer has recently been installed on Alcator C-Mod, complementing an existing 2.2 m grazing incidence Rowland circle spectrometer. These tools are currently used to support tokamak operations by monitoring a range of low-, mid- and high-Z impurities and study turbulent impurity transport by observing time-evolving emission from a new laser-blow off system. In addition, research in atomic processes in plasmas can be explored and the effect of charge-exchange on the high-n Lyman series is shown as an example.

VI. ACKNOWLEDGMENTS

The authors would like to thank Henry Savelli for engineering support and Tommy Toland and Patrick Scully for assistance with UHV hardware. This work supported by DOE Contact number DE-FC0299ER54512 and DE-AC52-07NA-27344

VII. REEFERENCES

[1]E. S. Marmar. Fusion Science and Technology. **51** 261 (2007)
[2]M. A. Graf, *et al*. Rev. Sci. Instrum. **66** 636 (1995)
[3]J. E. Rice, *et al*. J. Phys. B: At. Mol. Opt. Phys. **29** 2191 (1996)
[4]P. Beiersdorfer, *et al*. Rev. Sci. Instrum. **79** 10E318 (2008)
[5]M. B. Chowdhur, *et al*. Applied Optics. **47** 135 (2008)
[6]N. Yamaguchi, *et al*. Rev. Sci. Instrum. **65** 3408 (1994)
[7]J. Irby, *et al*. Fusion Science and Technology. **51** 460 (2007)
[8]T. Pütterich, J. Phys. B: At. Mol. Opt. Phys. **38** 3071 (2005)
[9]B. Lipschultz, *et al*. Phys. Plasmas. **13** 056117 (2006)
[10]N. Howard, *et al*. to be submitted to RSI (2010)
[11]J.K . Lepson, *et al*. The Astrophysical Journal. **590** 604 (2003)
[12]R. L. Kelly. Phys. Chem. Ref. Data. **16** 1 (1987)
[13]M. Mattiloi, *et al*. Phys. Rev. A. **40** 3886 (1989)
[14]L. F. Errea *et al*. Plasma Phys. Control. Fusion. **48** 1585 (2006)
[15]M. G.K. O' Mullane, *et al*. Plasma. Phys. Control. Fusion. **41** 105 (1999)
[16]K. D. Marr, *et al*. Plasma Phys. Control. Fusion. **52** 055010 (2010)

Iso-Sequence	Transition	WAVELENGTH [Å] Ar	Ca
Li-like	$2s_{1/2} - 3p_{3/2+1/2}$	23.529	18.694
Li-like	$2p_{1/2} - 3d_{3/2}$	24.864	19.646
Li-like	$2p_{3/2} - 3d_{5/2+3/2}$	25.024	19.790
Li-like	$2p_{1/2} - 3s_{1/2}$	25.548	20.129
Li-like	$2p_{3/2} - 3s_{1/2}$	25.700	20.296
Be-like	$2s^2_{1/2} - 2s3p_{3/2+1/2}$	24.740	19.558
Be-like	$2s_{1/2}2p_{3/2} - 2s_{1/2}3d_{5/2}$	25.927	20.439
Be-like	$2s_{1/2}2p_{3/2} - 2s_{1/2}3d_{3/2}$	27.044	21.200
Be-like	$2s_{1/2}2p_{3/2} - 2s_{1/2}3s_{1/2}$	28.340	22.113
B-like	$2s^22p_{1/2} - 2s^23d_{3/2}$	27.469	21.440
B-like	$2s^22p_{3/2} - 2s^23d_{5/2+3/2}$	27.631	21.609

Table 1: List of bright L-shell transitions in Li-, Be- and B-like isoelectronic sequences of Ar and Ca

FIGURE 1: Example spectra from the Rowland circle spectrometer showing the routinely measured molybdenum lines (black) and overlap during a tungsten injection (purple).

FIGURE 2: L-shell Ar spectrum measured during an Ohmic plasma with lines identification from EBIT. Emission from Li-, Be- and B-like lines are the dominate.

FIGURE 3: The change in the spectrum after a CaF_2 injection into an ICRF-heated L-mode. L-shell Ca spectral features match those shown in Figure 3 for Ar and K-shell F emission is also observed.

FIGURE 4: Time history of the line brightnesses over the time period of the injection showing a different time history for Ca XVIII coming from the core and F IX coming from the edge. The spectrum shown in FIGURE 4 is averaged over the highlighted region.

FIGURE 5: H- and He-like boron spectrum typical of Ohmic plasmas. The Lyman series is shown to not drop off monotonically at high-n where Ly_γ is brighter than Ly_β.

FIGURE 6: H- and He-like nitrogen spectrum in a ICRF L-mode plasma showing a similar high-n Lyman series enhancement but shifted so that Ly_δ is brighter than Ly_γ.

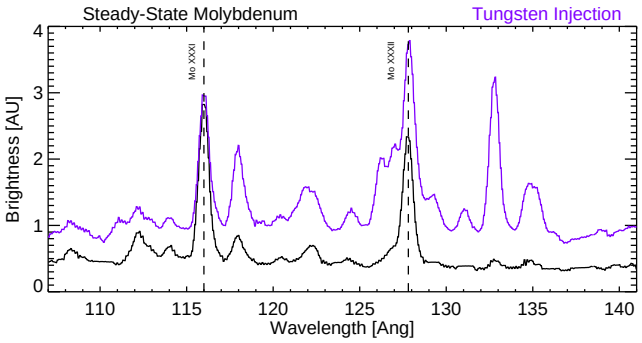

FIGURE 1

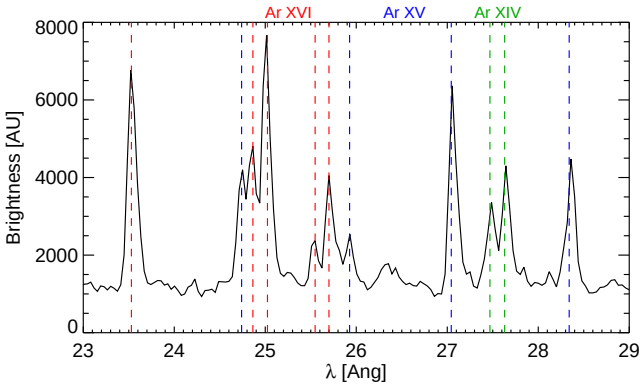

FIGURE 2

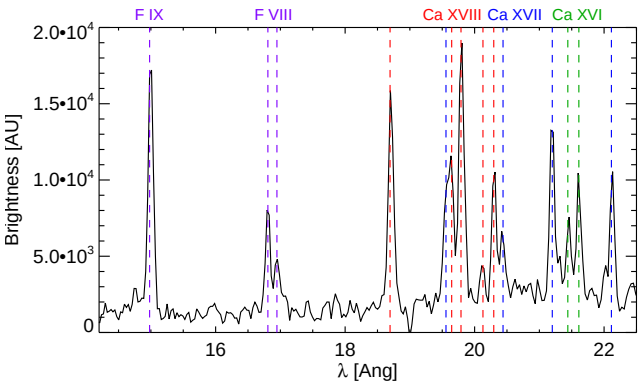

FIGURE 3

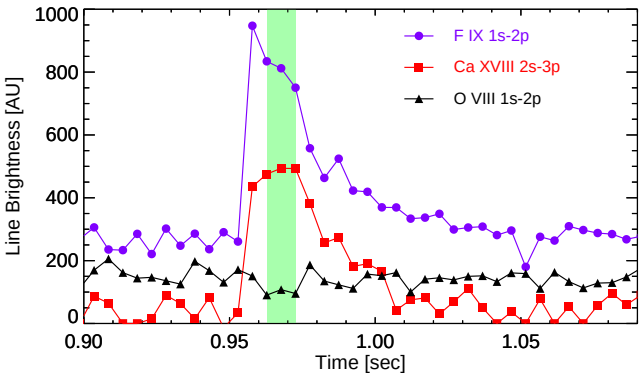

FIGURE 4

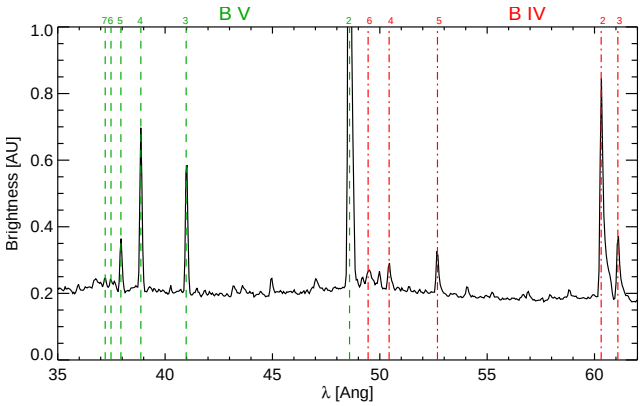

FIGURE 5

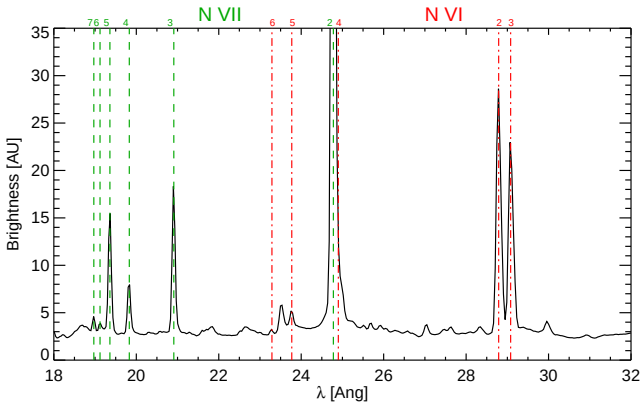

FIGURE 6